Journal of Engineering Science and Technology
Vol. 17, No. 5 (2022) 3254 - 3266

THE INFLUENCE OF INFILL DENSITY AND PATTERN ON THE MECHANICAL AND FRACTURE BEHAVIOR OF 3D PRINTED STRUCTURE SUBJECTED TO UNIAXIAL TENSILE LOAD

FARID TRIAWAN[1*], DEBBY SYEFIRA[1], MIA RISMALIA[1], IKA OKTAVIA SURYANI[1], DJATI WIBOWO DJAMARI[1], BENTANG ARIEF BUDIMAN[2], ASEP BAYU DANI NANDIYANTO[3]

[1]Department of Mechanical Engineering, Faculty of Engineering and Technology, Sampoerna University, Jl. Raya Pasar Minggu No. 16, Jakarta, Indonesia
[2]Faculty of Mechanical and Aerospace Engineering, Institut Teknologi Bandung, Jl. Ganesha No. 10, Bandung, Indonesia
[3]Departemen Kimia, Universitas Pendidikan Indonesia, Jl. Setiabudi No. 229, Bandung, Indonesia
*Corresponding Author: farid.triawan@sampoernauniversity.ac.id

Abstract

This study provides an investigation on the influence of 3D printing parameters, i.e., infill density and pattern, on the mechanical and fracture behavior of 3D printed structures. The specimens were fabricated using the Fused Deposition Modeling (FDM) method with infill density variation of 15, 25, 50, and 75% and infill pattern variation of the concentric, grid, and trihexagonal. The mechanical behavior of the specimens was tested by tensile test method and analytical observation of the specimen's fracture shape was performed. The result shows that increasing infill density could increase Young's modulus and ultimate tensile strength of the specimens. Moreover, the concentric infill pattern always exhibits the highest Young's modulus and ultimate tensile strength value compared to the grid and trihexagonal infill patterns. Based on the fracture shapes, the concentric infill pattern shows almost a flat fracture surface that is perpendicular to the applied tensile stress, confirming the brittle fracture mode. On the other hand, variations of fracture shape angle are found in the grid and trihexagonal infill pattern specimens. This might be due to the shifting direction of the maximum normal stress following the infill pattern direction. However, as the infill density reaches 75%, all specimens regardless of its infill pattern show a flatter fracture surface. Hence, the effect of infill pattern could be minimized if the infill density is near to 100%.

Keywords: 3D printing, FDM method, Fracture behavior, Infill density and pattern, Mechanical properties.

1. Introduction

Additive manufacturing or 3D printing is defined as the process of joining materials to produce a structural object from Computer-Aided Design (CAD) models. The ability of 3D CAD software in measuring multiple cross-sections allows the object to be printed precisely layer by layer [1]. It makes a variety of shapes of objects that can be produced, including the complex ones that are suited for customized products or functional prototypes [2]. The exploration of new material printability also has started to meet the demand for products with complexity and multi-functionality. For these reasons, the use of 3D printing to produce various products continues to increase and provides an ever-growing possibility of practical application. The method of producing 3D printed objects also has been progressed to fulfil the increasing demand of the complex structure product with a fine resolution [3].

The main methods introduced in 3D printing are Fused Deposition Modeling (FDM), Powder Bed Fusion (PBF), Stereolithography (SLA), and Direct Energy Deposition (DED). Among those methods, FDM is the preferred method to produce 3D printed objects. This method has been used in various applications, including automotive, aeronautics, construction, and medicine for rapid prototyping [4]. This method uses the thermoplastic polymer that is heated as the filament to print the layers. With high speed, simplicity, and low cost, FDM has become the method of choice for 3D printed objects.

Despite its promising application, the fiber orientation, bonding between the fiber and matrix, and the void formation still become a challenge that influences the mechanical properties of the 3D printed object [5]. The same consideration was also applied in the FDM method, mechanical weaknesses are mainly caused by the inter-layer distortion [6].

Another drawback of FDM methods was the layer-by-layer appearance, limitation on the thermoplastic material, and poor surface quality [7]. Optimizing mechanical properties through the modification of printing parameters (i.e., printing orientation, infill pattern, infill density, printing speed, nozzle temperature, and raster angle) has been reported by the previous study (see Table 1). The previous research summarized in Table 1 has shown favourable results in enhancing the 3D printed object's mechanical properties. Thus, further study is required to identify the critical and optimum printing parameters to enhance the quality of 3D printed objects.

In regard to the structure of 3D printed objects, it was reported that the infill density and pattern are both directly related to material strength [8]. To address this problem, based on our previous studies on the design of materials [9-20], this study investigates further the influence of infill density and pattern variations on the tensile properties and fracture behavior of the 3D-printed specimen made of Polylactic Acid (PLA) filament. The FDM method was chosen among many other methods by considering its advantages in high speed, simplicity, and low cost.

The specimens were printed with combinations of three infill patterns (grid, trihexagonal, and concentric) at multiple infill densities ranging from 15, 25, 50, to 75%. The tensile test results along with the fracture shapes were then analysed to identify how the infill density and pattern influence the mechanical properties.

Table 1. Summary of the previous studies on 3D printed object printing parameters.

Printing parameter	Result	Ref.
Infill density and pattern of PLA specimen fabricated using FDM method	Tensile properties are increased with increasing infill density. Concentric infill patterns have high tensile properties compared to the grid and trihexagonal infill patterns.	[8]
Layer thickness and infill density of PLA specimen	Maximum values of 3D printed material properties were achieved with a combination of 100% infill density with 0.1 mm layer thickness.	[21]
Nozzle temperature, raster angle, and air gaps of the specimen	The ultimate tensile strength of 3D printed objects was significantly affected by air gaps, while temperature and raster pattern did not bring significant results.	[22]
Build orientation and layer thickness of PLA specimen	For upright build orientation, increasing layer thickness could increase the flexural and tensile strength. While for on-edge and flat orientation, tensile and flexural strength are different, depending on the layer thickness.	[23]
Infill density of rectangular pattern 3D printed object	A rectangular pattern with a 90° deposition angle shows that increasing infill density leads to increase mechanical strength.	[24]
Layer thickness and infill density of 3D printed specimen	The maximum flexural force was affected by the layer thickness, while the flexural force deposition angle was affected by the infill density.	[25]
Infill density, feed rate, and infill pattern of 3D printed specimen	Increasing infill density increases the mechanical properties of the specimens. However, feed rate and infill pattern did not significantly influence the specimen's mechanical properties.	[26]

2. Material and Method

2.1. Specimen fabrication

Anycubic i3 Mega Extruder with open-source slicer software Ultimaker Cura 3.0 was used to control the printing parameter during the fabrication process of the specimens. The fabrication of the specimen followed the ASTM D638-Type I standard dimension, as shown in Fig. 1. The material chosen was 1.75 mm CCTREE 3D Printer ST-PLA Filament. The strength, affordability, and availability are the main consideration of using PLA material for fabricating the specimens [27]. Further details on the printing parameter used to fabricate the specimen are shown in Table 2.

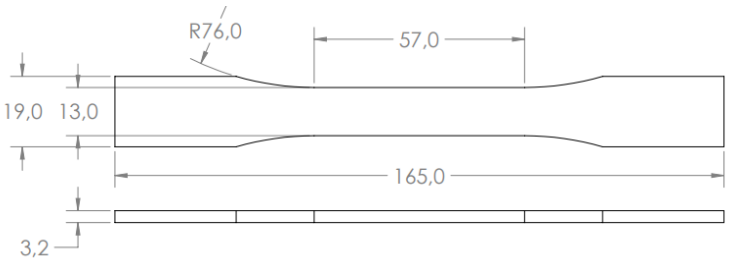

Fig. 1. ASTM D638-Type I standard of the specimen dimension in mm.

Table 2. Printing parameters of the specimens [18].

Parameters	Values
Layer height	0.1 mm
Thickness of wall	1.2 mm
Top and bottom thickness	0.6 mm
Printing temperature	210 ℃
Printing speed	50 mm/s
Plate temperature	70 ℃

The specimens were fabricated at three different infill patterns: grid, trihexagonal, and concentric as shown in Fig. 2 with 3-5 samples for each infill pattern variation. The grid pattern as shown in Fig. 2(a) prints the structure with 90°crossing paths and creates 45° angle with the XY axis. Trihexagonal pattern as shown in Fig. 2(b) prints the structure at angle of 120° with respect to each path. While the concentric pattern as shown in Fig. 2(c) prints the structure in the longitudinal axis in the same direction as the applied tensile load. Moreover, the infill density is varied into 15, 25, 50, and 75% with 3-5 samples for each infill density variation (Fig. 3).

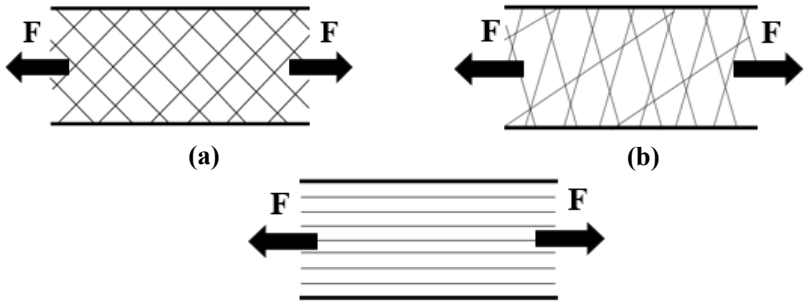

Fig. 2. Specimen infill pattern variation; (a) Grid, (b) Trihexagonal, (c) Concentric, with tensile load (F) direction.

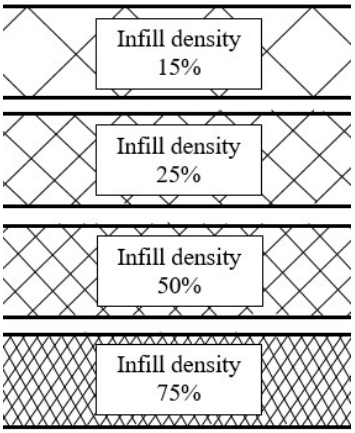

Fig. 3. Specimen infill density variation for the grid pattern.

2.2. Tensile test

Mechanical behavior of 3D printed structure was observed using Tensile test. Universal Testing Machine, Test Resource 313 with a 50 kN force transducers capacity was used to test the specimen at a 5 mm/min rate. The test was conducted following ASTM D638, which provides a standard method to test the plastic's tensile properties. The obtained data of uniaxial load was used to calculate the engineering stress by dividing the applied load with the specimen's cross-section area. The strain gauge attached to the specimen is used to get the engineering strain data by measuring the specimen's elongation. The strain data was automatically recorded using LabView software that is connected with the National Instruments data acquisition system, NI-9265. The strain gauge was then connected with the National Instruments data acquisition system, NI-9265, along with the LabView software to automatically record the strain data. Data resulting from the tensile test was then further analysed to obtain Young's modulus and ultimate tensile strength values. The ultimate tensile strength value was obtained by referring to the peak of the engineering stress-strain curve.

For Young's modulus, it was determined by evaluating the peak value of the tangent modulus of the stress-strain curve, which is considered as the slope of the curve for every strain increment, $\Delta\sigma/\Delta\varepsilon$ [28]. To comprehend the fracture behavior, observation on the fracture shape of each specimen was done by Ezren EZ-0234 USB Digital Microscope. The fracture angle was then compared to understand how infill pattern and density affect the fracture behavior of the specimens.

3. Results and Discussion

3.1. Stress and strain curves

Figure 4 plots the stress-strain curves of the concentric specimens with different infill densities. It can be observed that increasing infill density leads to an increasing trend in the stress-strain curve. Higher infill density allows a higher amount of PLA incorporated into the specimen; thus, it makes the specimen becomes less porous (more solid). This condition makes the specimen has a bigger cross-section area which contributes to increasing the tensile strength. As a result, the specimen does not easily break under the applied load. It tends to elongate in a higher stress value. On the other hand, the lower infill density only allows a smaller amount of PLA incorporated into the specimen, which makes the specimen become more porous. This causes the specimen to experience a higher stress value under the same applied load, which eventually makes it easier to break.

Figure 5 represents the stress-strain curve of a 3D printed structure with a variation of infill pattern at 50% infill density. The variation of the stress-strain value, in this case, is related to the type of infill pattern of the specimen. The experiment revealed that the concentric infill pattern exhibited higher stress-strain values compared to the grid and trihexagonal infill patterns. Referring to the printing orientation, the concentric infill pattern has the same alignment with the direction of the applied tensile load. Thus, it allows a higher force to hold by the specimen before experiencing fractures. Meanwhile, the grid and trihexagonal infill patterns have a different alignment with the applied load. This makes the applied load could not be uniformly distributed to the whole specimen body. It causes the specimens to be weaker than the concentric pattern. Moreover, due to the different

directions between the applied load and infill pattern, the stress concentration phenomenon is expected to generate locally in the specimen body, which leads to early plastic deformation, followed by crack initiation in the specimen body. As a result, the stress-strain curve of the grid and trihexagonal patterns are below the concentric pattern and behave similarly as shown in Fig. 5.

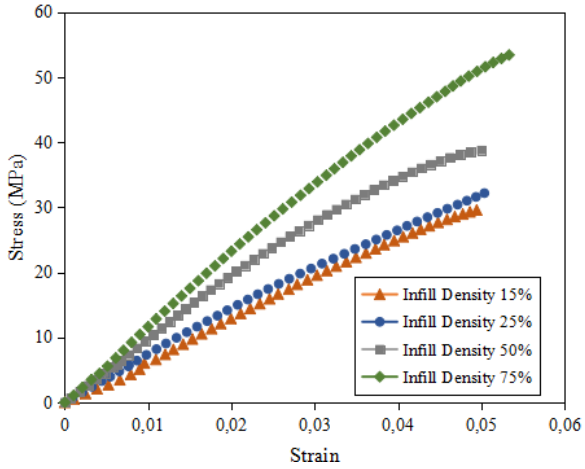

Fig. 4. Stress-strain curve of the concentric specimens with infill density variation.

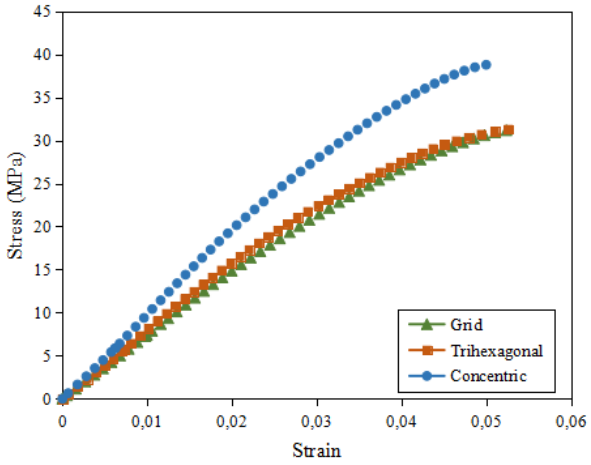

Fig. 5. Stress-strain curve of the specimens with infill pattern variation at 50% infill density.

3.2. Young's modulus

Young's modulus value was determined from the peak value of the tangent modulus of the stress-strain curve, which is considered as the slope of the curve for every strain increment. Figure 6 demonstrates the determination of Young's modulus for the concentric specimen with 50% infill density from the peak value of the slope curve. Table 3 summarizes all Young's moduli of all specimens.

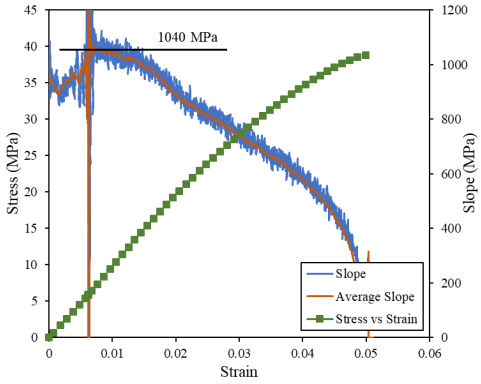

Fig. 6. Determination of Young's modulus value of concentric specimen at 50% infill density from the highest slope of the stress-strain curve.

The plot of Young's modulus values including the error bar for each specimens can be seen in Fig.7. However, as the standard deviation value is too small, the error bar added in Fig.7 cannot be seen clearly. From Fig. 7, it is found that increasing infill density results in increasing Young's modulus value. Increasing infill density allows the bonding between different sections of the infill pattern to increase. It results in higher stress needed to deform the specimen. While the different increasing trends are mainly affected by the printing process and the bonding between the printing layers. On the other hand, Young's modulus at the same infill density shows that the concentric infill pattern exhibits the highest value compared to the grid and trihexagonal infill pattern. The same direction of concentric infill pattern and the applied tensile load allows the load to be distributed across the specimen's body. It results in limiting the deformation under the same applied load, thus giving a higher Young's modulus value. Furthermore, Young's modulus values of the grid and trihexagonal patterns exhibited almost similar values. This indicates that both patterns give a similar effect on modifying the specimen deformation. However, a different trend is shown by the 15% grid infill density. It has a higher Young's modulus value compared to the trihexagonal infill pattern and has a closer value to the concentric pattern specimen. This might be affected by the large porosity effect for the 15% infill density that makes the structural stiffness among the three patterns did not differ significantly.

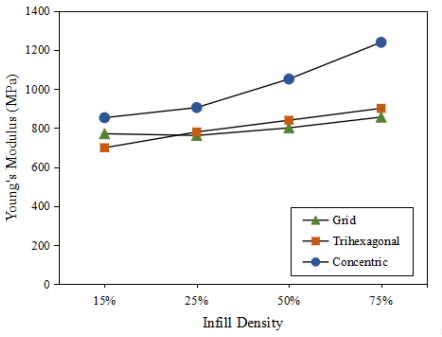

Fig. 7. Young's modulus of the specimens with infill pattern and density variation.

3.3. Ultimate tensile strength

The ultimate tensile strength of each specimen was defined from the peak of the stress-strain curve. The average ultimate tensile strength from 3-5 specimens along with the standard deviation can be seen in Table 3, while the plot and the error bar are shown in Fig. 8. From Fig. 8 it can be noticed that the ultimate tensile strength value increases with increasing infill density, where the 75% infill density exhibits the highest value while the 15% infill density has the lowest value.

Table 3. Young's modulus and ultimate tensile strength value of all specimens.

Infill pattern	Infill density	Young's modulus (MPa)	Ultimate tensile strength (MPa)
Grid	15%	771 ± 0.55	26.08 ± 0.93
	25%	762 ± 0.19	28.18 ± 1.32
	50%	801 ± 0.40	31.53 ± 0.87
	75%	856 ± 0.13	35.41 ± 1.26
Trihexagonal	15%	699 ± 0.60	28.87 ± 2.69
	25%	780 ± 0.18	28.08 ± 1.06
	50%	840 ± 0.11	30.53 ± 1.13
	75%	901 ± 0.10	36.80 ± 0.71
Concentric	15%	853 ± 0.17	29.84 ± 1.40
	25%	905 ± 0.39	33.53 ± 0.74
	50%	1051 ± 0.80	41.90 ± 2.59
	75%	1239 ± 0.14	42.09 ± 0.77

An increase in ultimate tensile strength for higher infill density is directly related to the amount of PLA in the specimen. The higher infill density allows a higher amount of PLA material incorporated into the specimens. The specimen becomes more solid and not easily be broken under the applied load. It also has a higher cross-section area which generates smaller internal stress under applied load. Meanwhile, the specimen with a lower infill density that has a lower cross-section area will generate higher internal stress under applied load. This causes the specimen to quickly deform plastically. The stress condition could be worsened when a stress concentration is generated locally at the joint of thin walls of the infill pattern, which will be the origin of crack initiation, and finally the specimen breaks.

The variation of the ultimate tensile strength value is also related to the infill pattern type. The experiment revealed that the concentric infill pattern exhibits the highest strength compared to the grid and trihexagonal infill patterns. The same alignment of concentric infill pattern with the applied load causes not only the higher structural stiffness (elastic modulus) but also increases the strength value. The whole applied load can be supported by the infill pattern; thus, the concentric pattern specimen is stronger than the other two patterns. While for the grid and trihexagonal infill patterns, the unparalleled direction of the infill pattern with the applied load causes the specimen not able to hold the applied load optimally, thus it decreases the strength. Like Young's modulus values, both the grid and trihexagonal patterns exhibit similar values of ultimate tensile strength, except for the infill density at 15%. The trihexagonal pattern shows a higher value of strength than the grid pattern and a closer value to the concentric pattern. This may be caused by the large porosity effect in which the variation of mechanical properties is expected [28].

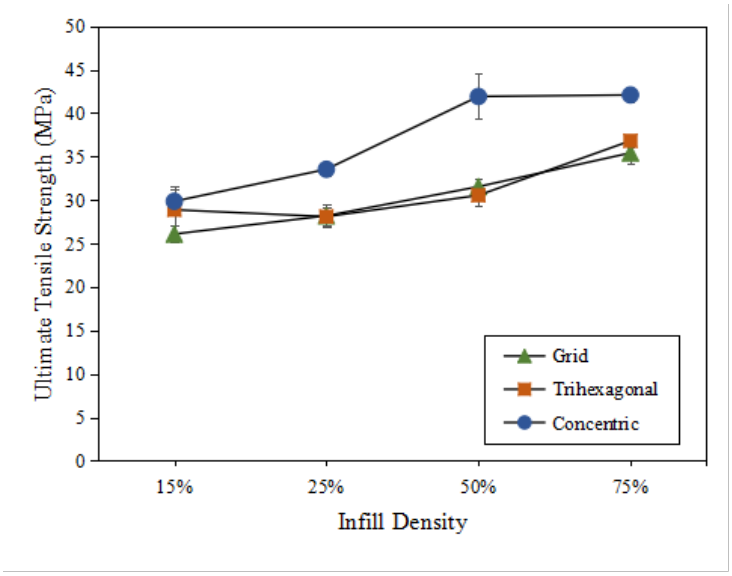

Fig. 8. Ultimate tensile strength of the specimens with infill pattern and density variation.

3.4. Fracture analysis of the specimens

Specimen fracture after undergoing tensile test was further analysed in terms of its fracture angle, as can be seen in Fig. 9. Generally, a brittle material that is uniaxially loaded in tension until it exceeds the strength, the material will fracture catastrophically with a flat fracture surface. The fracture direction is expected to be perpendicular with the maximum tensile stress direction (the principal stress). This is because brittle materials fail under normal stress, which explains the fracture shape of all specimens with concentric patterns in Fig. 9(a) that have a fracture angle of around 0°. On the other hand, the variations of fracture angles owned by the specimens with grid and trihexagonal patterns (see Fig. 9(b) and (c)) were likely affected by the direction of its infill pattern.

The direction of the maximum normal stress could be shifted following the infill pattern direction. In a concentric pattern, the infill pattern direction is aligned with the applied load; thus no shifting of direction is expected. However, in the grid and trihexagonal patterns, the infill pattern direction is not aligned with the applied load; thus the maximum normal stress may not be in the same direction as the applied load. This would create a stress concentration locally in the specimen body during testing, crack is then initiated and propagated at a certain angle, adjusting with the direction of the infill pattern inside the specimen body. This is likely the reason for the similar mechanical properties between specimens with grid and trihexagonal patterns (see Figs. 7 and 8).

As the infill density increases, the infill pattern becomes less effective in modifying the maximum normal stress direction because the specimen is more solid. Thus, the fracture surfaces of all specimens from the three patterns show flatter shapes relative to those of lower density. In Fig. 9, all specimens in 75% density show an almost flat fracture shape.

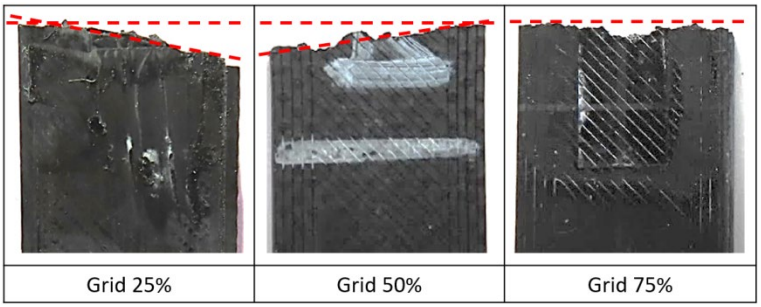

(a)

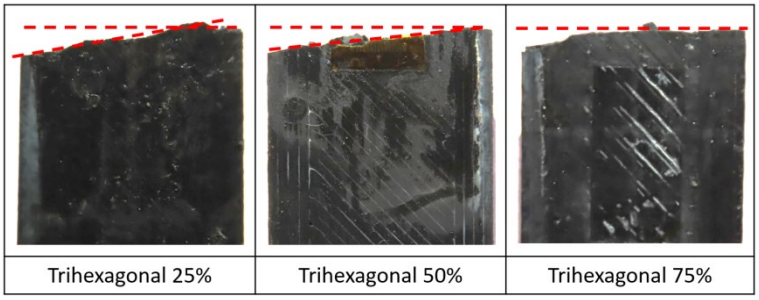

(b)

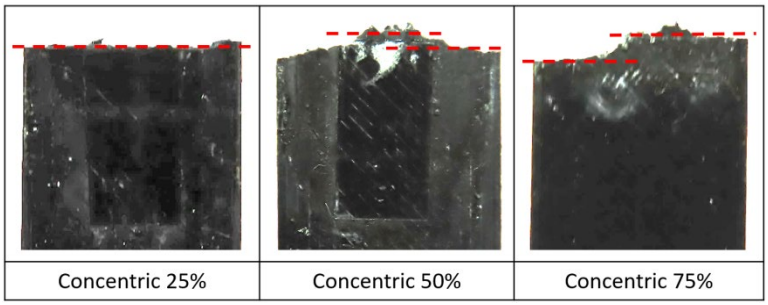

(c)

Fig. 9. Fracture shape of specimens with different infill patterns and densities; (a) Grid, (b) Trihexagonal, (c) Concentric.

4. Conclusion

The role of the printing parameters, i.e., infill density and pattern, in determining the mechanical properties and fracture behavior of 3D printed objects have been investigated in this work. The 3D printed specimens were fabricated by the FDM method using Polylactic Acid (PLA) materials. Infill density is related to the amount of plastic filament incorporated inside the specimen body. Higher infill density allows a higher amount of plastic incorporated into the specimen. This makes the specimen have fewer void spaces (porosity) which results in higher Young's modulus and ultimate tensile strength values. Infill pattern variation used in this study has shown that concentric exhibit better mechanical properties compared to the grid and trihexagonal infill patterns. In the concentric specimen,

the same direction of the infill pattern and the applied load affects the force distribution across the specimen's body. It results in higher structural stiffness (elastic modulus) and increases strength. While for other infill patterns, the different direction of infill pattern with the applied load causes the specimen not able to hold the applied load optimally and generate local stress concentration in the specimen body. As a result, the strength is not as high as the concentric infill pattern. Moreover, fracture shape analyses revealed that concentric infill pattern shows facture angle close to 0° (flat surface) regardless of the density, indicating the brittle failure mode. For the grid and trihexagonal infill patterns, the specimens fractured with an inclined fracture surface (not flat). This is likely affected by the shifting direction of the maximum normal stress following the infill pattern direction. The infill pattern effect could be minimized if the infill density is increased near to 100%. Under this condition, the principal stress would be in the same direction as the applied tensile load.

Acknowledgments

We acknowledged LPDP research grant, No. PRJ-85/LPDP/2020, and CRCS of Sampoerna University for providing generous financial and technical supports for running this research. A.B.D.N. acknowledged Ristek BRIN (Grant: Penelitian Terapan Unggulan Perguruan Tinggi) and Bangdos Universitas Pendidikan Indonesia.

References

1. Berman, B. (2012). 3-D printing: The new industrial revolution. *Business Horizons*, 55(2), 155-162.
2. Triawan, F.; Rachmawati, E.; Budiman, B.A.; Djamari, D.W.; Saputro, A.; and Arpi, I. (2021). Investigation of compressive behavior of pre-folded thin-walled column fabricated by 3D printing. *Indonesian Journal of Science and Technology*, 6(3), 543-560.
3. Ngo, T.D.; Kashani, A.; Imbalzano, G.; Nguyen, K.T.; and Hui, D. (2018). Additive manufacturing (3D printing): A review of materials, methods, applications and challenges. *Composites Part B: Engineering*, 143, 172-196.
4. Castiblanco, P.A.; Ramirez, J.L.; and Rubiano, A. (2021). Smart materials and their application in robotic hand systems: A state of the art. *Indonesian Journal of Science and Technology*, 6(2), 401-426.
5. Parandoush, P.; and Lin, D. (2017). A review on additive manufacturing of polymer-fiber composites. *Composite Structures*, 182, 36-53.
6. Sood, A.K.; Ohdar, R.K.; and Mahapatra, S.S. (2010). Parametric appraisal of mechanical property of fused deposition modelling processed parts. *Materials and Design*, 31(1), 287-295.
7. Mohamed, O.A.; Masood, S.H.; and Bhowmik, J.L. (2015). Optimization of fused deposition modeling process parameters: a review of current research and future prospects. *Advances in Manufacturing*, 3(1), 42-53.
8. Rismalia, M.; Hidajat, S.C.; Permana, I.G.R.; Hadisujoto, B.; Muslimin, M.; and Triawan, F. (2019). Infill pattern and density effects on the tensile properties of 3D printed PLA material. *Journal of Physics: Conference Series*, 1402(4), 044041.

9. Asriyanti, A.; Septiani, T.D.; Siagian, M.S.P.; and Triawan, F. (2021). Portable coffin lowering device for covid-19 corpse handling: education, design process, and strength analysis. *Indonesian Journal of Multidiciplinary Research*, 1(1), 41-54.
10. Khoiriyah, N.; Alfatih, S.A.; Munir, M.; and Triawan, F. (2021). Component design and strength analysis of coffin lowering machine for Covid-19 corpse: a problem-based learning. *Indonesian Journal of Multidiciplinary Research*, 1(1), 137-150.
11. Sineri, G.A.A.; Octary, A.V.; Ali, M.F.; Iza, N.R.; and Triawan, F. (2021). Structural design and strength analysis of lifting machine for home appliance flood safety tool: A problem-based learning. *Indonesian Journal of Multidiciplinary Research*, 1(2), 159-170.
12. Muryanti, L.; Fitria, L.N.; Hanaya, G. and Triawan, F. (2021). Foldable bed design concept for covid-19 patient: A machine design case study. *ASEAN Journal of Science and Engineering*, 1(2), 113-126.
13. Pingak, C.T.R.; Octaviani, M.A.; Yuenan, G.C. and Triawan, F. (2022). Bed-stretcher for burial process of covid-19 corpse: A preliminary design and strength analysis. *ASEAN Journal of Science and Engineering*, 2(1), 105-114.
14. Qushai, I.L.A.; Sholeh, A.; Budiarta, W.N.; and Triawan, F. (2021). Motorcycle child seat for child with special needs: Its design process and problem-based learning. *Indonesian Journal of Community and Special Needs Education*, 1(2), 93-102.
15. Triawan, F.; Nandiyanto, A.B.D.; Abdullah, A.G.; and Aziz, M. (2018). Plasma nitriding time on the hardness and crystal structure/phase of SUS403 and SCS6 martensitic stainless steels: an analytical study. *Journal of Engineering Science and Technology*, 13(8), 2369-2378 (2018).
16. Triawan, F.; Nandiyanto, A.B.D.; Suryani, I.O.; Fiandini, M.; and Budiman, B.A. (2020). The influence of turmeric microparticles amount on the mechanical and biodegradation properties of cornstarch-based bioplastic material: From bioplastic literature review to experiments. *Materials Physics and Mechanics*, 46(1). 99-114.
17. Nandiyanto, A.B.D.; Hofifah, S.N.; Girsang, G.C.S.; Putri, S.R.; Budiman, B.A.; Triawan, F.; and Al-Obaidi, A.S.M. (2021). The effects of rice husk particles size as a reinforcement component on resin-based brake pad performance: From literature review on the use of agricultural waste as a reinforcement material, chemical polymerization reaction of epoxy resin, to experiments. *Automotive Experiences*, 4(2), 68-82.
18. Nandiyanto, A.B.D.; Triawan, F.; Fiandini, M.; Suryani, I.O.; and Sunnardianto, G.K. (2021). Influence of the size of turmeric microparticles reinforcing agent on mechanical and biodegradation properties of cornstarch-based bioplastic material: current studies, experimental results, and proposal material crack phenomena during mechanical testing. *Materials Physics and Mechanics*, 47(2), 266-284.
19. Nandiyanto, A.B.D.; Triawan, F.; Firly, R.; Kishimoto, K. (2021). Crystallite size on micromechanical characteristics of WO3 microparticles. *Journal of Engineering Research*, 9(3A), 268-277.

20. Triawan, F.; Aprilia, G.E.; Saptaji, K.; Saville, R.; and Nandiyanto, A.B.D. (2021). Determining crispness level of dry food through its compressive strain energy. *Indonesian Journal of Computing, Engineering and Design* (*IJoCED*), 3(2), 106-118.
21. Torres, J.; Cotelo, J.; Karl, J.; and Gordon, A.P. (2015). Mechanical property optimization of FDM PLA in shear with multiple objectives. *Jom*, 67(5), 1183-1193.
22. Wu, W.; Geng, P.; Li, G.; Zhao, D.; Zhang, H.; and Zhao, J. (2015). Influence of layer thickness and raster angle on the mechanical properties of 3D-printed PEEK and a comparative mechanical study between PEEK and ABS. *Materials*, 8(9), 5834-5846.
23. Chacón, J.M.; Caminero, M.A.; García-Plaza, E.; and Núnez, P.J. (2017). Additive manufacturing of PLA structures using fused deposition modelling: Effect of process parameters on mechanical properties and their optimal selection. *Materials and Design*, 124, 143-157.
24. Abbas, T.; Othman, F.M.; and Ali, H.B. (2017). Effect of infill Parameter on compression property in FDM Process. *Dimensions*, 12(12.7), 25-4.
25. Lužanin, O.; Movrin, D.; and Plančak, M. (2014). Effect of layer thickness, deposition angle, and infill on maximum flexural force in FDM-built specimens. *Journal for Technology of Plasticity*, 39(1), 49-58.
26. Qattawi, A.; Alrawi, B.; and Guzman, A. (2017). Experimental optimization of fused deposition modelling processing parameters: A design-for-manufacturing approach. *Procedia Manufacturing*, 10, 791-803.
27. Tymrak, B.M.; Kreiger, M.; and Pearce, J.M. (2014). Mechanical properties of components fabricated with open-source 3-D printers under realistic environmental conditions. *Materials and Design*, 58, 242-246.
28. Triawan, F.; Kishimoto, K.; Adachi, T.; Inaba, K.; Nakamura, T.; and Hashimura, T. (2012). The elastic behavior of aluminum alloy foam under uniaxial loading and bending conditions. *Acta Materialia*, 60(6-7), 3084-3093.